Available online at www.sciencedirect.com
ScienceDirect
Journal of Solid State Chemistry 179 (2006) 3126–3135
JOURNAL OF SOLID STATE CHEMISTRY
www.elsevier.com/locate/jssc

Stuffed rare earth pyrochlore solid solutions

G.C. Lau*, B.D. Muegge, T.M. McQueen, E.L. Duncan, R.J. Cava

Department of Chemistry, Princeton University, Princeton, NJ 08544, USA

Received 23 March 2006; received in revised form 7 June 2006; accepted 9 June 2006
Available online 14 June 2006

Abstract

Synthesis and crystal structures are described for the compounds $Ln_2(Ti_{2-x}Ln_x)O_{7-x/2}$, where Ln = Tb, Dy, Ho, Er, Tm, Yb, Lu, and x ranges from 0 to 0.67. Rietveld refinements of X-ray powder diffraction data indicate that in the Tb and Dy titanate pyrochlores, the extra Ln^{3+} cations mix mainly on the Ti^{4+} site with little disorder on the original Ln^{3+} site. For the smaller rare earths (Ho–Lu), stuffing additional lanthanide ions results in a pyrochlore to defect fluorite transition, where the Ln^{3+} and Ti^{4+} ions become completely randomized at the maximum ($x = 0.67$). Initial magnetic characterization for the fully stuffed $x = 0.67$ samples for Ln = Tb–Yb shows no long range ordering down to 2 K, and only partial saturation of the full expected magnetic moment under applied fields up to 5 T. In all of these Ln–Ti–O pyrochlores, the addition of magnetic Ln^{3+} in place of non-magnetic Ti^{4+} adds edge sharing tetrahedral spin interactions to a normally corner sharing tetrahedral network of spins. The increase in spin connectivity in this family of solid solutions represents a new avenue for investigating geometrical magnetic frustration in the rare earth titanate pyrochlores.

Keywords: Pyrochlore; Stuffed pyrochlore; Stuffed spin ice; Geometrically frustrated magnet; Pyrochlore to fluorite solid solution; Rare earth titanate

1. Introduction

Pyrochlore materials, with general formula $A_2B_2O_7$, represent an important structure type in view of geometrical magnetic frustration due to the ordering of the A and B cations into separate interpenetrating lattices of corner sharing tetrahedra. Spins of magnetic atoms placed in either lattice position can result in frustration, where the presence of many energetically equivalent ground states suppresses long-range ordering of the moments [1]. Unusual low-temperature physics as a consequence of magnetic frustration has been seen in the well-studied rare earth pyrochlores including cooperative paramagnetism in $Tb_2Ti_2O_7$ [2–5] and spin ice characteristics in $Dy_2Ti_2O_7$ [6–10] and $Ho_2Ti_2O_7$ [11–16]. Novel magnetic states as a result of frustration are also seen in $Y_2Ru_2O_7$ [17,18] and the superconducting β-pyrochlore $RbOs_2O_6$ [19]. Most studies focusing on magnetic frustration in pyrochlores are based on magnetic moments isolated on either the A or B-site, with spin interactions becoming more complicated when the different cations are both magnetic [20,21]. While the effect of decreasing the magnetic lattice connectivity through diluting the magnetic atom with non-magnetic species on the same site has been explored [5,22,23], there have not been, to our knowledge, examples of increasing this connectivity by "stuffing" more of the same magnetic atom onto the non-magnetic site.

Stuffing more A cations onto the B-site in pyrochlores can lead to disordering of the separate corner-sharing tetrahedral networks. This disordering, or cation mixing, typically occurs only in pyrochlores with larger B cations, such as Zr^{4+} [24–27]. For the rare earth titanate pyrochlores, due to the large difference in size between Ln^{3+} and Ti^{4+} ions, mixing of cations in the $Ln_2Ti_2O_7$ stoichiometry has only been reported under conditions such as ball milling, ion irradiation, or reduction with CaH_2 [28–30]. Stuffed cubic phases of titanates, in the form $Ln_2(Ti_{2-x}Ln_x)O_{7-x/2}$ are reported for Ln = Dy–Lu, but only at limited stuffing levels with the focus on these materials as oxygen ionic conductors [31–37]. According to the early phase diagrams, a wider range of Ln^{3+} stuffing is possible for cubic titanates of the smaller lanthanides (Ho–Lu) at high temperatures, but these stoichiometries

*Corresponding author.
E-mail address: glau@princeton.edu (G.C. Lau).

0022-4596/$ - see front matter © 2006 Elsevier Inc. All rights reserved.
doi:10.1016/j.jssc.2006.06.007

are difficult to obtain as different crystal structures are more thermodynamically stable at lower temperatures [38–44].

Here we report the synthesis and crystal structures determined by X-ray powder diffraction of polycrystalline $Ln_2(Ti_{2-x}Ln_x)O_{7-x/2}$, where Ln = Tb–Lu and x ranges from 0 to 0.67. Initial magnetic characterization is also reported here for the fully stuffed $x = 0.67$ end members: Ln_2TiO_5, with Ln = Tb–Yb. These solid solutions in the Ln_2O_3–TiO_2 systems contain Ln/Ti ratios ranging from 1, in the original pyrochlore, to 2 in the fully stuffed materials. The occupation of magnetic Ln^{3+} ions in either A or B-site is determined with respect to the stuffing level, illustrating the structural evolution in these compounds as the connectivity in the magnetic spins is increased. The placing of additional spins in the corner-sharing tetrahedral network potentially opens a new window in the study of rare earth titanates in light of geometrical magnetic frustration [45].

2. Experimental

To synthesize $Ln_2(Ti_{2-x}Ln_x)O_{7-x/2}$ (Ln = Tb–Lu), stoichiometric amounts of rare earth oxides (Tb_4O_7, Johnson Matthey, 99.9%; Dy_2O_3, Alfa Aesar, 99.9%; Ho_2O_3, Alfa Aesar, 99.9%; Er_2O_3, Alfa Aesar, 99.99%; Tm_2O_3, Alfa Aesar, 99.9%; Yb_2O_3, Aldrich, 99.9%; Lu_2O_3, Alfa Aesar, 99.99%) and TiO_2 (Aldrich,99.9%) were intimately ground and pressed into pellets. For Ln = Ho–Lu, samples were heated in a static argon atmosphere at 1700 °C for 12 h, and quenched in a water-cooled furnace chamber to room temperature in approximately 30 min. Stuffed titanates with Tb and Dy were made by arc-melting 100 mg sized pellets of the mixed binary oxides to allow for faster quenching of the samples. No pre-reaction was required in the arc-melted samples.

The crystal structures were characterized through X-ray powder diffraction (XRD) using a Bruker D8-Focus employing Cu$K\alpha$ radiation with a diffracted beam monochromator. The software TOPAS 2.1 (Bruker AXS) operated in the fundamental parameters approach was used for Rietveld structure refinements. All patterns were refined in space group *Fd-3 m* (No. 227) with the origin placed on the 16*c* site (*B*-site). Ln^{3+} and Ti^{4+} occupancies were allowed to refine freely on both the *A* and *B*-sites of the pyrochlore, with the constraint that their total occupancies from both sites maintained the nominal stoichiometric ratios. Oxygen occupation on both the 8*b* and 8*a* sites was allowed to refine with the constraint that the total occupancy on both sites summed to maintain charge neutrality in the compound as there was no indication of lower oxidation state Ti in any of the phases. The oxygen thermal parameters were fixed at reasonable values, given the well-known insensitivity of the XRD powder refinement method to the details of the oxygen array in heavy ion compounds. In addition to the parameters shown in Table 1, other refined parameters include background, zero error correction, scaling factor,

Table 1
Crystallographic parameters for the series $Ln_2(Ti_{2-x}Ln_x)O_{7-x/2}$ in space group *Fd-3 m* (No 227)

Ln/ Parameter		x 0	0.1	0.2	0.3	0.4	0.5	0.67
Tb								
	a (Å)	10.1694(2)	10.1928(2)	10.2317(2)	10.2575(2)	—	—	10.4022(8)
x pos.	48*f*	0.3287(7)	0.3278(7)	0.3290(8)	0.3318(9)	—	—	0.349(2)
Ti^{4+} Occ.	16*d*	0.035(3)	0.013(3)	0.035(4)	0.029(4)	—	—	0.065(8)
	16*c*	0.965(3)	0.937(3)	0.865(4)	0.821(4)	—	—	0.605(8)
O^{2-} Occ.	8*b*	1	0.94(1)	0.87(2)	0.78(2)	—	—	0.49(3)
	8*a*	0	0.01(1)	0.03(2)	0.07(2)	—	—	0.18(3)
B_{eq}	16*d*	0.46(5)	0.51(4)	0.94(7)	0.84(7)	—	—	1.1(2)
	16*c*	0.9(1)	1.0(1)	1.9(1)	1.6(1)	—	—	1.4(2)
	R_{wp}	12.01	12.71	12.38	11.78	—	—	13.56
	χ^2	1.11	1.17	1.14	1.12	—	—	1.23
Dy								
	a (Å)	10.136(1)	10.1622(2)	10.1946(2)	10.2262(3)	10.2715(4)	10.3084(5)	10.3614(6)
x pos.	48*f*	0.3194(8)	0.3265(8)	0.3319(8)	0.3343(8)	0.341(1)	0.336(1)	0.349(2)
Ti^{4+} Occ.	16*d*	0.036(3)	0.019(3)	0.018(3)	0.030(4)	0.042(5)	0.050(6)	0.101(8)
	16*c*	0.964(3)	0.931(3)	0.882(3)	0.821(4)	0.758(5)	0.700(6)	0.569(8)
O^{2-} Occ.	8*b*	1	0.95(1)	0.90(2)	0.83(2)	0.73(2)	0.64(3)	0.63(4)
	8*a*	0	0.00(1)	0.00(2)	0.02(2)	0.07(2)	0.11(3)	0.04(4)
B_{eq}	16*d*	0.26(5)	0.18(4)	0.59(5)	0.87(7)	1.1(1)	0.6(1)	0.4(2)
	16*c*	0.8(1)	0.9(1)	1.2(1)	1.4(1)	1.4(2)	0.6(2)	0.4(2)
	R_{wp}	11.62	10.78	10.91	10.81	12.31	12.31	12.42
	χ^2	1.15	1.09	1.12	1.12	1.13	1.11	1.13
Ho								
	a (Å)	10.1048(2)	10.133(2)	10.163(2)	10.1958(5)	10.2302(4)	10.2575(3)	10.3058(3)

Table 1 (*continued*)

Ln/ Parameter		x = 0	0.1	0.2	0.3	0.4	0.5	0.67
x pos.	48*f*	0.3294(5)	0.3271(5)	0.3264(6)	0.3336(6)	0.3361(6)	0.3444(9)	0.3367(8)
Ti^{4+} Occ.	16*d*	0.016(3)	0.014(3)	−0.030(3)	−0.002(4)	0.032(4)	0.116(6)	0.351(8)
	16*c*	0.984(3)	0.936(3)	0.930(3)	0.852(4)	0.768(4)	0.634(6)	0.320(8)
O^{2-} Occ.	8*b*	1	0.937(1)	0.90(1)	0.79(1)	0.74(1)	0.57(2)	0.70(2)
	8*a*	0	0.013(9)	0.00(1)	0.06(1)	0.06(1)	0.18(2)	−0.03(2)
B_{eq}	16*d*	0.83(4)	1.17(4)	0.63(9)	1.31(7)	2.05(8)	1.8(2)	0.8(2)
	16*c*	1.37(9)	1.61(8)	0.41(9)	1.0(1)	0.9(1)	0.3(2)	1.2(2)
	R_{wp}	9.81	8.82	9.62	9.69	9.69	9.79	10.53
	χ^2	1.18	1.10	1.12	1.11	1.21	1.23	1.26
Er								
	a (Å)	10.076(3)	10.116(6)	10.132(9)	10.164(3)	10.2002(3)	10.2222(4)	10.2663(3)
x pos.	48*f*	0.3283(5)	0.3296(6)	0.3311(5)	0.3321(7)	0.3344(6)	0.347(1)	0.355(2)
Ti^{4+} Occ.	16*d*	0.031(2)	0.009(3)	0.004(2)	0.045(3)	0.029(3)	0.146(5)	0.32(3)
	16*c*	0.969(2)	0.941(3)	0.896(2)	0.805(3)	0.771(3)	0.604(5)	0.35(2)
O^{2-} Occ.	8*b*	1	0.95(1)	0.89(1)	0.68(1)	0.68(1)	0.51(2)	0.66(8)
	8*a*	0	0.00(1)	0.01(1)	0.17(1)	0.12(1)	0.24(2)	0.01(8)
B_{eq}	16*d*	1.07(4)	2.26(5)	1.72(5)	1.79(7)	3.42(9)	0.8(1)	0.5(5)
	16c	2.2(1)	2.3(1)	1.8(1)	2.9(1)	1.7(1)	0.8(1)	0.3(5)
	R_{wp}	7.99	8.04	7.73	7.91	7.75	7.94	7.95
	χ^2	1.21	1.18	1.22	1.17	1.22	1.19	1.20
Tm								
	a (Å)	10.054(1)	10.0843(4)	10.1104(4)	10.1338(4)	10.1595(2)	10.1846(5)	10.2245(5)
x pos.	48*f*	0.3261(5)	0.3300(7)	0.3291(7)	0.3318(7)	0.3331(8)	0.347(1)	0.338(1)
Ti^{4+} Occ.	16*d*	0.002(2)	−0.029(3)	−0.010(3)	−0.010(3)	0.026(3)	0.137(5)	0.322(9)
	16*c*	1.002(2)	0.979(3)	0.910(3)	0.860(3)	0.774(3)	0.613(5)	0.349(9)
O^{2-} Occ.	8*b*	1	0.89(1)	0.83(1)	0.77(1)	0.72(2)	0.55(2)	0.64(5)
	8*a*	0	0.06(1)	0.07(1)	0.08(1)	0.08(2)	0.20(2)	0.03(5)
B_{eq}	16*d*	0.23(3)	0.16(3)	0.48(4)	0.65(4)	0.88(5)	1.2(1)	1.6(2)
	16*c*	0.72(8)	0.21(9)	0.55(9)	0.44(9)	0.35(9)	0.1(1)	0.8(2)
	R_{wp}	8.85	9.44	9.24	9.28	9.25	10.65	9.56
	χ^2	1.27	1.22	1.18	1.24	1.20	1.45	1.27
Yb								
	a (Å)	10.0327(1)	10.056(1)	10.082(2)	10.102(3)	10.127(2)	10.1557(2)	10.1881(2)
x pos.	48*f*	0.3231(5)	0.3259(6)	0.3321(7)	0.3311(7)	0.3426(8)	0.349(1)	0.341(1)
Ti^{4+} Occ.	16*d*	−0.016(2)	−0.026(2)	−0.008(3)	−0.021(3)	0.078(3)	0.252(9)	0.329(8)
	16*c*	1.016(2)	0.976(2)	0.908(3)	0.871(3)	0.722(3)	0.498(9)	0.341(8)
O^{2-} Occ.	8*b*	1	0.95(1)	0.85(1)	0.82(1)	0.69(2)	0.49(3)	0.67(4)
	8*a*	0	0.00(1)	0.05(1)	0.03(1)	0.11(2)	0.26(3)	0.00(4)
B_{eq}	16*d*	0.52(3)	1.32(3)	1.52(4)	1.07(4)	1.61(6)	1.5(2)	1.5(2)
	16*c*	0.68(9)	1.06(9)	1.3(1)	0.42(9)	1.02(9)	0.3(2)	1.2(2)
	R_{wp}	11.59	10.01	10.05	11.72	12.72	11.27	11.28
	χ^2	1.34	1.17	1.15	1.28	1.44	1.22	1.28
Lu								
	a (Å)	10.0197(2)	—	—	10.0864(3)	—	—	10.1683(4)
x pos.	48*f*	0.3250(6)	—	—	0.3335(8)	—	—	0.340(1)
Ti^{4+} Occ.	16*d*	0.019(2)	—	—	0.035(3)	—	—	0.324(8)
	16*c*	0.98(2)	—	—	0.815(3)	—	—	0.346(8)
O^{2-} Occ.	8*b*	1	—	—	0.77(2)	—	—	0.67(4)
	8*a*	0	—	—	0.08(2)	—	—	0.00(4)
B_{eq}	16*d*	0.39(3)	—	—	1.33(6)	—	—	1.7(2)
	16*c*	1.3(1)	—	—	1.4(1)	—	—	1.2(2)
	R_{wp}	10.14	—	—	10.75	—	—	10.89
	χ^2	1.24	—	—	1.41	—	—	1.49

Ln^{3+} and Ti^{4+} both refined on 16d (1/2, 1/2, 1/2) and 16*c* (0, 0, 0) sites. O^{2-} placed on 8*b* (3/8, 3/8, 3/8), 8a (1/8, 1/8, 1/8), and 48f (*x*, 1/8, 1/8) sites.

and crystal size and strain. For the case of the arc-melted samples, which had well-developed crystallites, a preferred orientation parameter was included in the refinements.

Magnetic characterization of the fully stuffed, Ln_2TiO_5, samples was performed using a Quantum Design PPMS magnetometer. Magnetic susceptibilities of these

polycrystalline samples were measured under an applied field of 1 kOe in the temperature range 2–280 K. Field dependence of the magnetization for the six fully stuffed pyrochlores was measured at 5 K under applied fields of up to 5 T.

3. Results and discussion

In general, the thermodynamic phase diagrams [38–42,46–48] between the compositions $Ln_2Ti_2O_7$ and Ln_2TiO_5 show full two phase regions between the fixed composition end members, with hexagonal and orthorhombic stable ordered phases at room temperature in ordered Ln_2TiO_5. Disordered high-temperature fluorite type Ln_2TiO_5 [38–42,46] and limited solid solutions [44] are reported for Dy–Lu lanthanides. In the current study, however, the solid solution series, $Ln_2(Ti_{2-x}Ln_x)O_{7-x/2}$ (Ln = Tb-Lu, $0 \leqslant x \leqslant 0.67$), were successfully synthesized as single phase materials through high-temperature synthesis followed by rapid quenching. Quenching allowed for the bypassing of more thermodynamically stable lower temperature phases or phase separation into rare earth richer and poorer phases. $Ln_2(Ti_{2-x}Ln_x)O_{7-x/2}$ solid solutions based on the smaller lanthanides (Ho–Lu), with Ln^{3+} closer in size to Ti^{4+}, formed with a slower quench (30 min to room temperature from 1700 °C) whereas stuffed pyrochlore titanates based on Tb and Dy, the largest successful cases, required arc melting to cool more quickly.

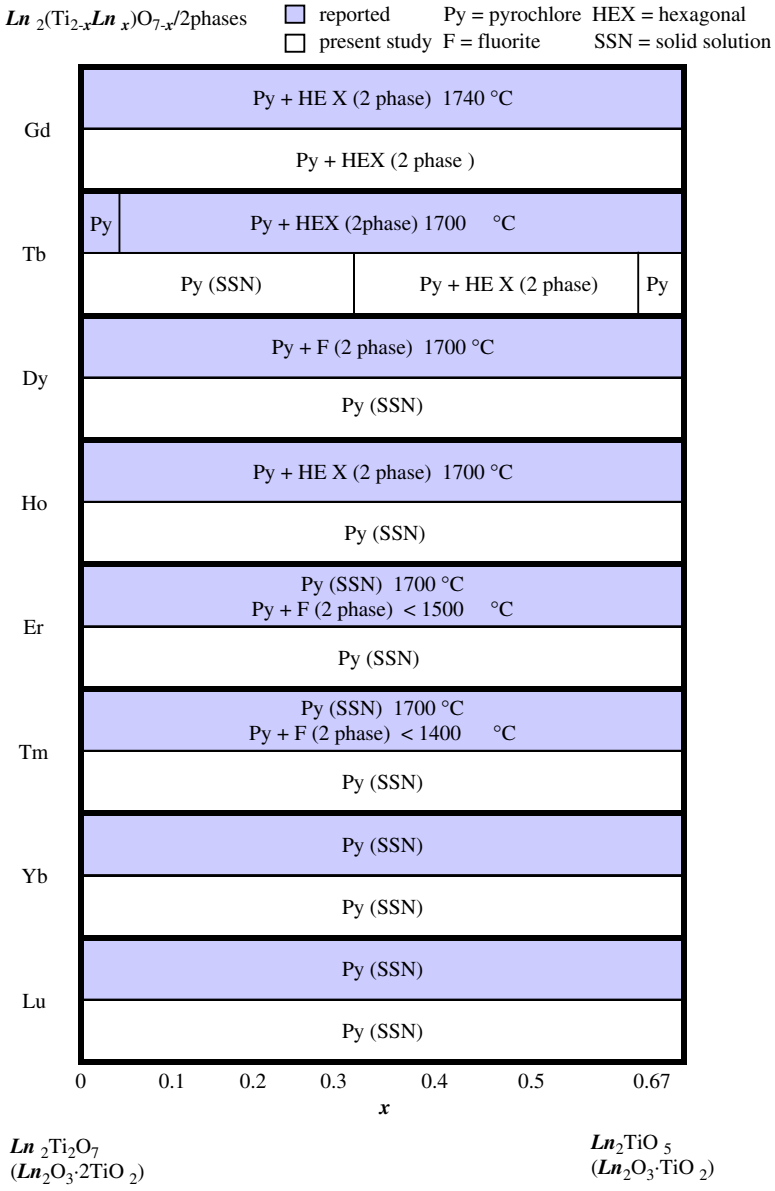

Fig. 1. Phase diagrams for each $Ln_2Ti_2O_7$–Ln_2TiO_5 system (Ln = Gd–Lu), comparing known high temperature phases [38–42,46–48] (upper rows) with those found in this study (lower rows). Pyrochlore (P) $Ln_2Ti_2O_7$ with either ordered hexagonal (HEX) or disordered fluorite (F) Ln_2TiO_5 two phase regions are seen for many of the larger lanthanides. Pyrochlore solid solutions, P (SSN), are formed at 1700 °C except for the Tb and Dy cases, where the series are quenched from the melt (>1800 °C).

The $x = 0.4$ and 0.5 samples in the Tb series were never successfully formed as pure single phases, having the more stable, ordered hexagonal symmetry phase also present. In the Gd–Ti–O system and for larger lanthanides, even the fast cooling rates attained in arc melting could not stabilize any substantial stuffing level in the cubic pyrochlore structure. This difficulty in forming the stuffed solid solutions for the larger rare earths is consistent with the expectation that ions with large size differences (i.e. large Ln^{3+} and Ti^{4+}) will tend not to mix on the same site. Simplified phase diagrams comparing the high-temperature phases known in the literature [38–42,46–48] with those found in this study for each rare earth titanate are presented in Fig. 1.

The final refined structural parameters for all the stuffed pyrochlores studied are presented in Table 1 as fits to a cubic pyrochlore structure. The weighted residuals (R_{wp}) and goodness of fit parameters (χ^2) indicate that the structural models are excellent representations of the structures. For the smaller rare earths, Ho–Lu, a smooth pyrochlore to defect fluorite transition is seen as a function of stuffing. As shown in Fig. 2, with $Ho_2(Ti_{2-x}Ho_x)O_{7-x/2}$ as an example, the $x = 0$ non-stuffed pyrochlore begins with ordered corner-sharing tetrahedral lattices of both Ho^{3+} and Ti^{4+}. The magnetic Ho^{3+} atoms on the *A*-site form a distinct network separated from the non-magnetic Ti^{4+} on the *B*-site by a crystallographic offset of (1/2, 1/2, 1/2), yet the two sublattices are exactly equivalent in size and atomic distances. As more Ho^{3+} is added in the range $0 \leqslant x \leqslant 0.3$, Ho^{3+} replaces Ti^{4+} strictly on the *B*-site (Table 1), developing edge-sharing tetrahedral spin interactions outlined in green. Above $x = 0.4$, Ti^{4+} begins to mix onto the originally pure Ho^{3+} 16d site. At $x = 0.67$, the maximally doped sample has complete mixing of Ho^{3+} and Ti^{4+} so that the *A* and *B*-sites are indistinguishable from each other. The lack of cation ordering reduces the pyrochlore superstructure to the smaller unit cell sized fluorite structure. The X-ray data for the $x = 0.67$ samples for Ln = Ho–Lu confirm this disorder through the absence of the (1 1 1), (3 1 1) and (3 3 1) pyrochlore superstructure peaks. The pyrochlore structure can still be used to describe these maximally stuffed end members (weighted residuals of fits using pyrochlore or fluorite structures are nearly equal), and is thus presented in Table 1 to more clearly show the trends in increasing lattice parameter and cation disorder. The oxygen atoms are not considered in detail in the present work due to the relative insensitivity of our powder XRD method to that information. The role of oxygen in stabilizing the pyrochlore to fluorite structure transition is well described in previous reports [24,49,50]. Future studies by neutron diffraction designed to determine the manner in which the oxygen ion distribution changes during the pyrochlore to fluorite transition in these phases will be of considerable interest.

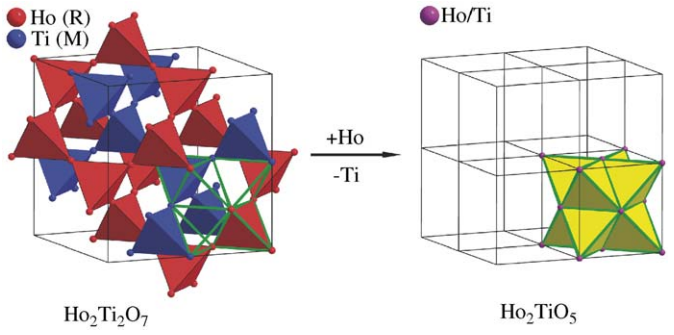

Fig. 2. A simplified model of the original pyrochlore, $Ho_2Ti_2O_7$ (left), and the transition to a fluorite crystal structure (right) in the series $Ho_2(Ti_{2-x}Ho_x)O_{7-x/2}$. Ho (red) and Ti (blue) form separate corner sharing tetrahedral lattices in the pyrochlore structure, but develop edge-sharing connectivity (green line) as extra Ho is stuffed in place of Ti. At $x = 0.67$, Ho and Ti are completely mixed and can be represented in the fluorite structure as one site (purple) with disordered Ho/Ti in a 2:1 ratio. Oxygen atoms are omitted for clarity.

Fig. 3a illustrates the linear increase of the cubic pyrochlore lattice parameter, *a*, with excess lanthanide concentration, indicative of the successful stuffing of extra Ln^{3+} on the *B*-site in each series. The inset shows that the rates of increase in the unit cells (i.e. the slopes of *a* versus *x*) also change linearly with radius of the different rare earth cations (effective radii of Ln^{3+} ions in six-fold oxygen coordination as given by Shannon and Prewitt) [51]. At given compositions, *x*, the lattice parameters continue to generally follow a linear increase with lanthanide radius as shown in Fig. 3b.

Fig. 4 plots the Ti^{4+} occupation of the originally pure Ln^{3+} *A*-site as a function of Ln^{3+} doping, *x*. In the range $0 \leqslant x \leqslant 0.3$, all the lanthanides (Tb–Lu) show virtually no mixing within the experimental uncertainties associated with our XRD method. Above $x = 0.4$, the smaller Ho–Lu series show Ti^{4+} mixing continuously and rapidly onto the *A*-site to about a 30% level – the expected disordered ratio in the fluorite structure with chemical composition Ln_2TiO_5. For Tb and Dy, the *A*-site mixing increases slightly ($<10\%$) but never reaches the fully disordered level required in fluorite, and thus a pyrochlore-like structure (although disordered) is maintained through $x = 0.67$ stuffing. Fig. 5 shows an example of one of the observed and calculated powder XRD patterns for one of the small lanthanide (Ho) stuffed pyrochlores, and the inset shows a detail of one of the diffraction peaks across the series, indicating the presence of good crystallinity.

Difficulties in synthesizing Tb and Dy-stuffed pyrochlores are represented in Fig. 6. The main panel shows a structure refinement of the $x = 0.1$ stuffed Dy titanate with sharp symmetric peaks of a well-crystallized polycrystalline material. However, upon further doping of extra Dy, the inset shows how the diffraction peaks become broader and asymmetric. The Tb patterns display the same characteristics. We interpret the broadening of the peaks to be a sign of compositional inhomogeneity in the samples caused by the thermodynamically driven phase separation to pyrochlore $Dy_2Ti_2O_7$ and lower-temperature phases of

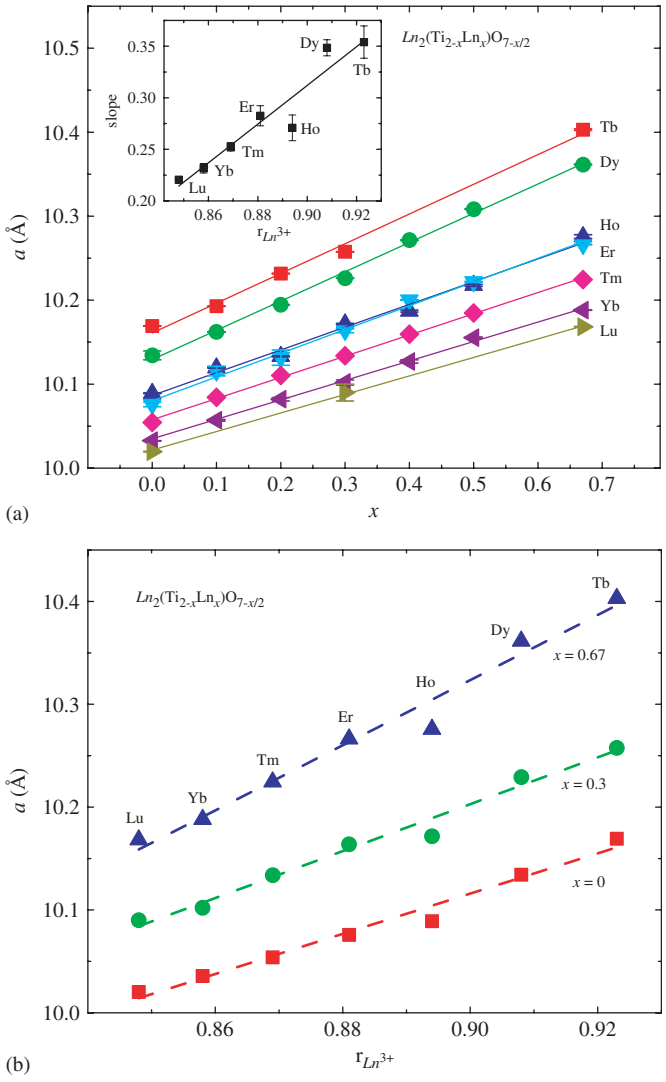

Fig. 3. (a) The lattice parameter, a, of the cubic pyrochlore materials, $Ln_2(Ti_{2-x}Ln_x)O_{7-x/2}$, with respect to stuffing level, x (main panel). Linear increase of the unit cell in each case reveals the effect of replacing Ti^{4+} with larger Ln^{3+} cations. Inset illustrates the slopes measured from the lattice parameter dependence on x (from main panel) plotted against the rare earth ionic radius. (b) The lattice parameter, a, at three different x compositions plotted versus lanthanide ion radius. Dotted lines show a generally linear increase of unit cell size with varying rare earths.

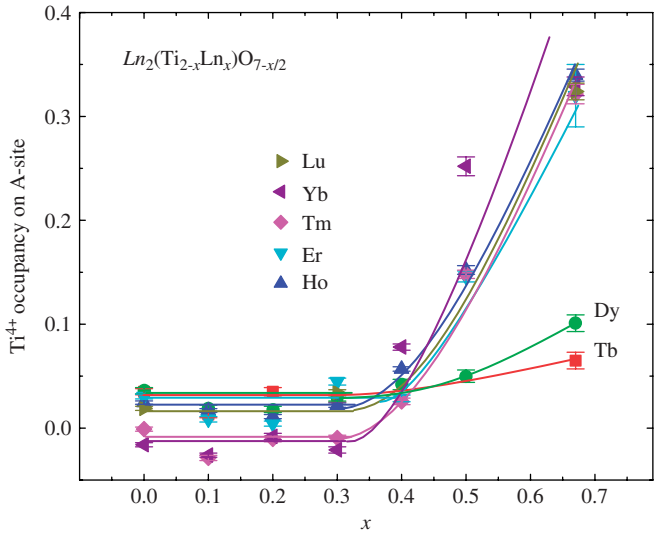

Fig. 4. Fraction of Ti^{4+} occupancy on the pyrochlore A-site is plotted versus stuffing level. The small fraction of Ti^{4+} mixing at low x is taken to be zero within experimental error of our method. No mixing on the A-site shows that the stuffed Ln^{3+} initially displaces Ti^{4+} on the B-site before mixing more thoroughly on both sites at higher x for Ln = Ho–Lu. Tb and Dy samples display low mixing on the A-site even at maximum stuffing.

Dy_2TiO_5. Samples cooled at slower rates in both resistance-heated and optical image floating zone furnaces resulted in the minor presence of hexagonal Dy_2TiO_5. An estimate of the spread in composition of the stuffed Tb and Dy samples can be made from the excess peak width and the variation of the peak position with average composition. The range in peak position was determined by the difference in full-width at half-maximum (FWHM) of the largest peak (2 2 2) between the $x = 0.67$ and 0 samples. The corresponding range in lattice parameter associated with this variation in peak position gives the spread in composition, x, through the linear fits used in Fig. 3a. The composition spread is estimated to be $\Delta x = 0.09$ for the maximally stuffed Tb sample and $\Delta x = 0.05$ for Dy. Difficulties in fitting the broadened peaks in this family did not significantly impact the determination of the metal atom mixing, which is the main structural characterization undertaken in the present study. The very large difference in sizes between Ln^{3+} and Ti^{4+}, even for the small lanthanides, makes the extensive occurrence of the stuffed pyrochlores surprising. To test for the possible presence of short range Ln–Ti ordering, preliminary electron diffraction study was undertaken for the $Dy_2(Ti_{2-x}Dy_x)O_{7-x/2}$ stuffed pyrochlores for $x = 0.2$ and 0.67. There was no indication of short range ordering of the Dy^{3+} and Ti^{4+} ions in the sample.

Fig. 7 displays the magnetic susceptibilities as $(\chi-\chi_0)^{-1}$(T) for the $x = 0.67$ end members in the $Ln_2(Ti_{2-x}Ln_x)O_{7-x/2}$ series with Ln = Tb–Yb. Due to the possibility of crystal field (CF) effects affecting the susceptibility [52–54], Curie–Weiss law fits [$\chi = \chi_0 + C/(T-\theta_W)$, where C is the Curie constant and χ_o is a temperature-independent contribution] to the susceptibilities were performed for both high and low-temperature ranges. The high-temperature (125–280 K for Ln = Tb–Tm, 150–280 K for Yb) portion of the $\chi(T)$ data was fit to determine χ_o, which ranged from 4×10^{-4} to 1×10^{-3} emu/mol$_{Ln}$Oe for Tb–Tm, with Yb giving -4×10^{-3} emu/mol$_{Yb}$ Oe. Curie-Weiss thetas, θ_W, and the effective moments, μ_{eff}, were determined from the linear fits of the two temperature ranges and are displayed in Table 2. From the high-temperature data, the determined effective moments in general agree well with the expected full

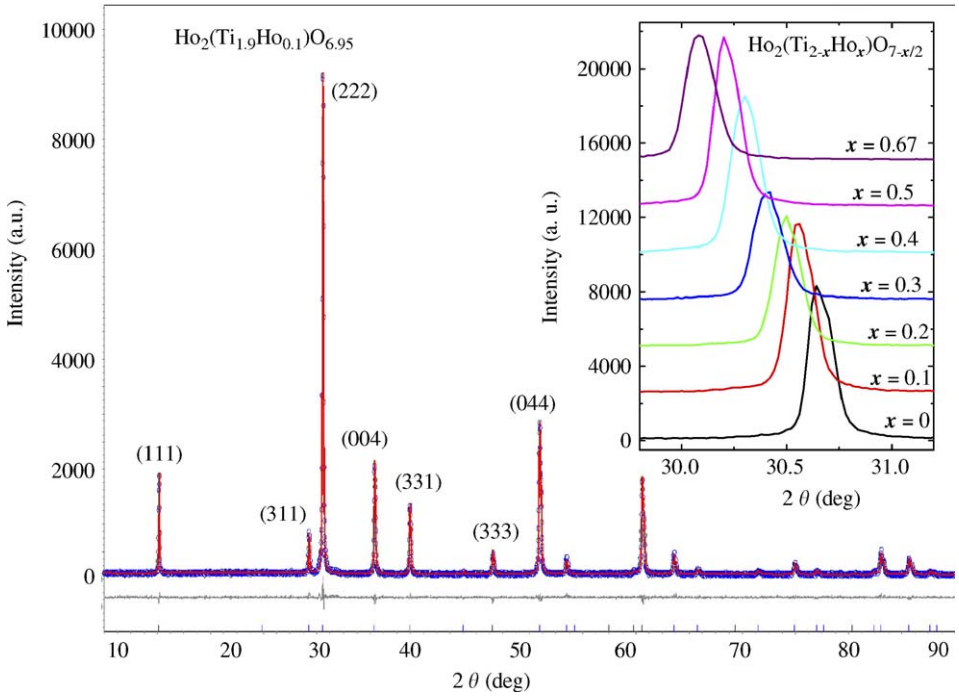

Fig. 5. Rietveld structure refinement of $Ho_2(Ti_{1.9}Ho_{0.1})O_{6.95}$ shown with raw data in blue, fitted pattern in red, and the difference in gray (main panel). Peak indices for the first 7 reflections in the pyrochlore structure are labeled. A magnified view of the (2 2 2) peak for each of the stuffed Ho titanates is shown in the inset.

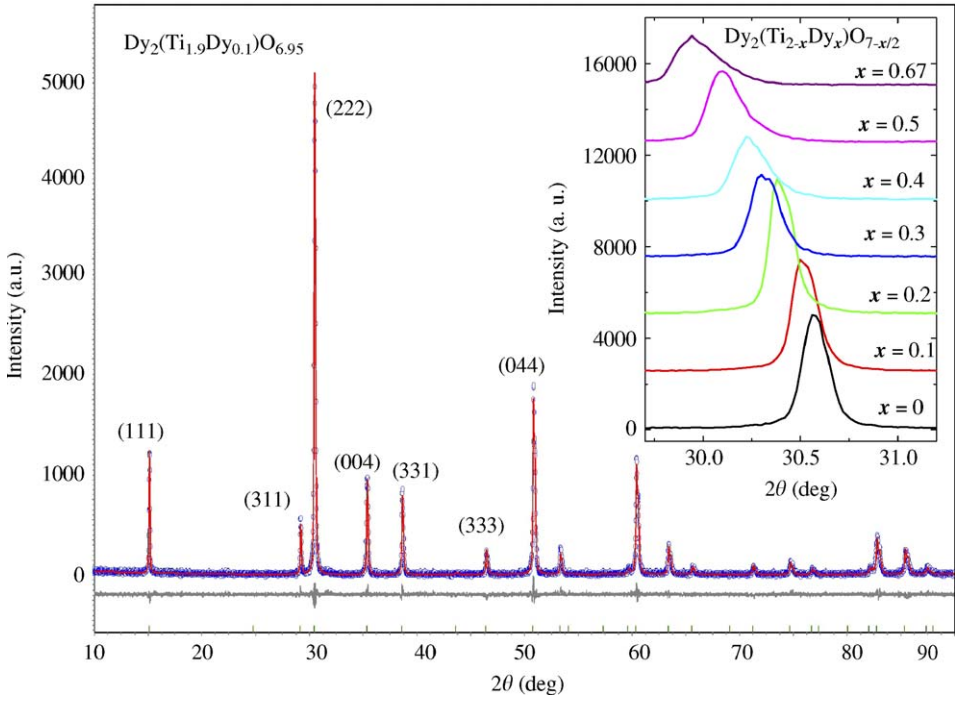

Fig. 6. Rietveld structure refinement of $Dy_2(Ti_{1.9}Dy_{0.1})O_{6.95}$ shown with raw data in blue, fitted pattern in red, and the difference in gray (main panel). Peak indices for the first 7 reflections in the pyrochlore structure are labeled. A magnified view of the (2 2 2) peak for each of the stuffed Dy titanates is shown in the inset. Peak broadening and asymmetry occur at higher levels of Dy stuffing.

moment of free Ln^{3+} ions, with the lower temperature data only giving slightly smaller μ_{eff}. The Yb sample is different than the other rare earths, giving the largest difference in Curie–Weiss values determined from the two temperature ranges indicating the possibility of significant CF effects in Yb_2TiO_5. The negative Curie–Weiss thetas of all

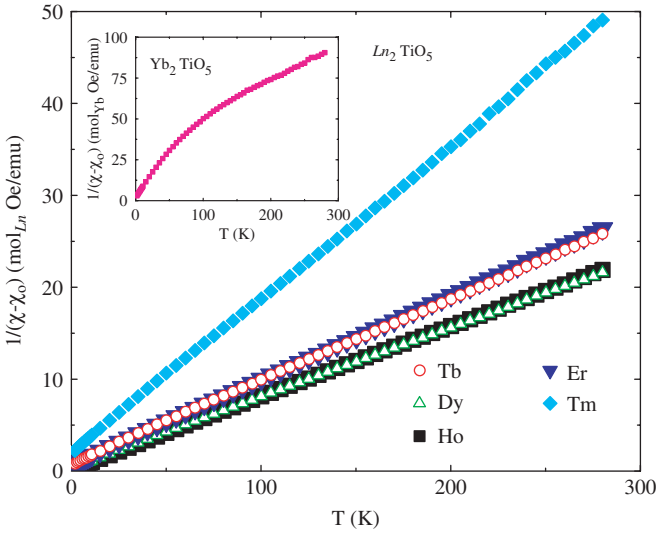

Fig. 7. Magnetic susceptibilities for the $x = 0.67$ members of the series $Ln_2(Ti_{2-x}Ln_x)O_{7-x/2}$ (Ln_2TiO_5) are measured in an applied field of 1 kOe and plotted here as inverse susceptibility versus temperature. Inset: the data for Yb_2TiO_5.

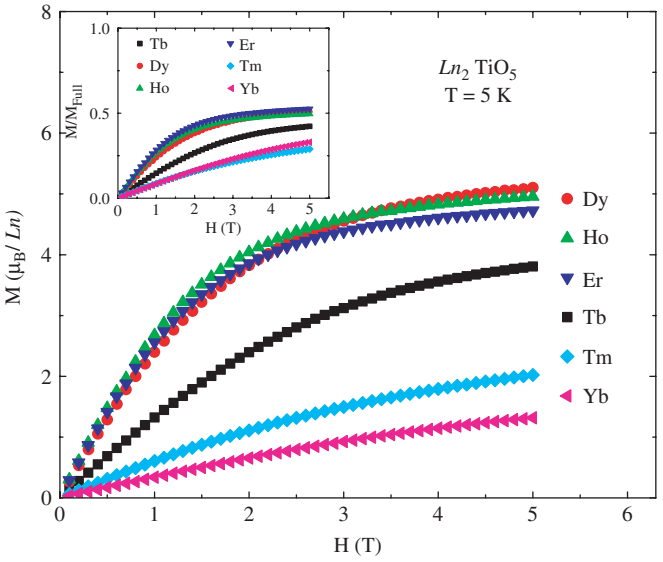

Fig. 8. Field dependence of the magnetization for the Ln_2TiO_5 samples measured at 5 K up to applied fields of 5 T is shown in the main panel for each fully stuffed rare earth titanate. The inset gives magnetizations normalized by the full number of Bohr magnetons expected for free Ln^{3+} ions. In each case, only half or less than half of the expected full magnetization is observed.

Table 2
Curie–Weiss constants and magnetic moments determined from the magnetic susceptibility for the $x = 0.67$ end members of $Ln_2(Ti_{2-x}Ln_x)O_{7-x/2}$

Compound	Fit range (K)	θ_W (K)	μ_{eff} Observed (μ_B)	μ_{eff} Expected (μ_B)
Tb_2TiO_5	2–50	−7.2(1)	9.07(6)	9.72
	125–280	−12.9(3)	9.54(2)	
Dy_2TiO_5	2–50	−3.3(1)	9.99(2)	10.63
	125–280	−9.0(3)	10.35(3)	
Ho_2TiO_5	10–50	−1.5(1)	9.97(5)	10.6
	125–280	−7.2(2)	10.26(2)	
Er_2TiO_5	10–50	−8.1(2)	9.23(9)	9.59
	125–280	−9.7(3)	9.38(2)	
Tm_2TiO_5	2–50	−11.6(1)	6.84(4)	7.57
	125–280	−22.1(5)	7.36(3)	
Yb_2TiO_5	2–50	−4.1(2)	3.71(5)	4.54
	150–280	−161(2)	6.24(7)	

Ln_2TiO_5 samples indicate predominantly antiferromagnetic interactions, in contrast with $Dy_2Ti_2O_7$ and $Ho_2Ti_2O_7$ which show weak ferromagnetic behavior [52]. However, in similarity to the spin ice pyrochlores, none of the Ln_2TiO_5 samples showed indication of long-range magnetic order down to 2 K. While the spin interactions are no longer limited to corner-sharing tetrahedra as in $Ln_2Ti_2O_7$, the new edge-sharing tetrahedral configuration that develops with stuffing is also a frustrating geometry. This, along with the considerable site disorder of the magnetic lanthanide atoms, should contribute to the suppression of long-range magnetic order.

Fig. 8 gives the field dependence of the magnetization of the Ln_2TiO_5 materials at 5 K up to fields of 5 T. Within our field range, none of the samples reached the full magnetization expected for free Ln^{3+} ions. Magnetizations of the Dy, Ho, and Er samples appear to begin saturating close to half of full magnetization, similar to bulk measurements seen on the parent $Ln_2Ti_2O_7$ compounds [52]. This suggests that despite the mixing of Ln^{3+} and Ti^{4+} in these site disordered materials, single-ion anisotropy similar to that in the ordered $Ln_2Ti_2O_7$ pyrochlores still remains. For Ln = Tb, Tm, and Yb, the 5 T magnetization is significantly less than half saturation, suggesting the mechanism behind the reduced magnetization is different than for Dy, Ho, and Er. More detailed magnetic measurements on all the samples in each lanthanide series would be of interest to better characterize the geometric frustration in these stuffed rare earth titanates.

4. Conclusions

We have successfully synthesized polycrystalline samples in a range of stuffed rare earth titanates, $Ln_2(Ti_{2-x}Ln_x)O_{7-x/2}$ (Ln = Tb–Lu, $0 \leqslant x \leqslant 0.67$) by high temperature synthesis and rapid cooling. We have analyzed their crystal structures and taken preliminary magnetic measurements on the fully stuffed end members. For the smaller lanthanides (Ho–Lu) a smooth pyrochlore to defect fluorite transition is observed as more Ln^{3+} ions are stuffed into the structure. Tb and Dy titanates are more difficult to stuff, given the larger size differences between

the Ln^{3+} and Ti^{4+} ions. This results in less mixing between the two cations, with disorder mostly on the *B*-site of the pyrochlore structure, but no complete transition to fluorite even at maximum stuffing. In all cases, the spin interactions limited to corner-sharing tetrahedra in the original pyrochlores are transformed to an edge-sharing tetrahedral geometry upon stuffing. The fully stuffed pyrochlores show antiferromagnetic behavior but with no long-range magnetic order down to 2 K. $M(H)$ data suggest that single-ion anisotropy of the Ln^{3+} cations exists in these fully stuffed titanates resulting in incomplete magnetization, similar to the $Ln_2Ti_2O_7$ pyrochlores. The ability to chemically alter the magnetic connectivity in these well-studied materials presents an opportunity to uncover more unusual behavior associated with geometrical magnetic frustration in future physical characterization.

Acknowlegdments

This work was supported by the National Science Foundation Division of Materials Research, and partly supported under a National Science Foundation Graduate Research Fellowship.

References

[1] M.J. Harris, M.P. Zinkin, Modern Phys. Lett. B. 10 (1996) 417–438.
[2] J.S. Gardner, S.R. Dunsiger, B.D. Gaulin, M.J.P. Gingras, J.E. Greedan, R.F. Kiefl, M.D. Lumsden, W.A. MacFarlane, N.P. Raju, J.E. Sonier, I. Swainson, Z. Tun, Phys. Rev. Lett. 82 (1999) 1012–1015.
[3] J.S. Gardner, A. Keren, G. Ehlers, C. Stock, E. Segal, J.M. Roper, B. Fak, M.B. Stone, P.R. Hammar, D.H. Reich, B.D. Gaulin, Phys. Rev. B. 68 (2003) 180401(R).
[4] I. Mirebeau, I.N. Goncharenko, J. Phys.-Condens. Matter. 17 (2005) S771–S782.
[5] B.G. Ueland, G.C. Lau, R.J. Cava, J.R. O'Brien, P. Schiffer, Phys. Rev. Lett. 96 (2006) 027216.
[6] R. Higashinaka, H. Fukazawa, Y. Maeno, Phys. Rev. B. 68 (2003) 014415.
[7] S.V. Isakov, R. Moessner, S.L. Sondhi, Phys. Rev. Lett. 95 (2005) 217201.
[8] A.P. Ramirez, A. Hayashi, R.J. Cava, R. Siddharthan, B.S. Shastry, Nature 399 (1999) 333–335.
[9] J. Snyder, J.S. Slusky, R.J. Cava, P. Schiffer, Nature 413 (2001) 48–51.
[10] J. Snyder, B.G. Ueland, J.S. Slusky, H. Karunadasa, R.J. Cava, P. Schiffer, Phys. Rev. B. 69 (2004) 064414.
[11] S.T. Bramwell, M.J.P. Gingras, Science 294 (2001) 1495–1501.
[12] S.T. Bramwell, M.J. Harris, B.C. den Hertog, M.J.P. Gingras, J.S. Gardner, D.F. McMorrow, A.R. Wildes, A.L. Cornelius, J.D.M. Champion, R.G. Melko, T. Fennell, Phys. Rev. Lett. 8704 (2001) 047205.
[13] A.L. Cornelius, J.S. Gardner, Phys. Rev. B. 64 (2001) 060406.
[14] G. Ehlers, A.L. Cornelius, T. Fennell, M. Koza, S.T. Bramwell, J.S. Gardner, J. Phys.-Condens. Matter 16 (2004) S635–S642.
[15] T. Fennell, O.A. Petrenko, B. Fak, J.S. Gardner, S.T. Bramwell, B. Ouladdiaf, Phys. Rev. B. 72 (2005) 224411.
[16] M.J. Harris, S.T. Bramwell, D.F. McMorrow, T. Zeiske, K.W. Godfrey, Phys. Rev. Lett. 79 (1997) 2554–2557.
[17] J.S. Lee, T.W. Noh, J.S. Bae, I.S. Yang, T. Takeda, R. Kanno, Phys. Rev. B. 69 (2004) 214428.
[18] J.S. Lee, T.W. Noh, T. Takeda, R. Kanno, Phys. B-Conden. Matter 359 (2005) 1240–1242.
[19] M. Bruhwiler, S.M. Kazakov, N.D. Zhigadlo, J. Karpinski, B. Batlogg, Phys. Rev. B. 70 (2004) 020503.
[20] J.S. Gardner, A.L. Cornelius, L.J. Chang, M. Prager, T. Bruckel, G. Ehlers, J. Phys.-Condens. Matter 17 (2005) 7089–7095.
[21] O. Sakai, Y. Jana, R. Higashinaka, H. Fukazawa, S. Nakatsuji, Y. Maeno, J. Phys. Soc. Jpn. 73 (2004) 2829–2833.
[22] J. Snyder, J.S. Slusky, R.J. Cava, P. Schiffer, Phys. Rev. B. 66 (2002) 064432.
[23] J. Snyder, B.G. Ueland, A. Mizel, J.S. Slusky, H. Karunadasa, R.J. Cava, P. Schiffer, Phys. Re. B. 70 (2004) 184431.
[24] M.A. Subramanian, G. Aravamudan, G.V.S. Rao, Progr. Solid State Chem. 15 (1983) 55–143.
[25] D. Michel, M. Perezyjo, R. Collongu, Materi. Res. Bull. 9 (1974) 1457–1468.
[26] H. Ohtani, S. Matsumoto, B. Sundman, T. Sakuma, M. Hasebe, Materi. Trans. 46 (2005) 1167–1174.
[27] M.J.D. Rushton, R.W. Grimes, C.R. Stanek, S. Owens, J. Mater. Res. 19 (2004) 1603–1604.
[28] A.F. Fuentes, K. Boulallya, M. Maczka, J. Hanuza, U. Amador, Solid State Sci 7 (2005) 343–353.
[29] J. Lian, L. Wang, J. Chen, K. Sun, R.C. Ewing, J.M. Farmer, L.A. Boatner, Acta Mater 51 (2003) 1493–1502.
[30] G.D. Blundred, C.A. Bridges, M.J. Rosseinsky, Angew. Chem.-Int. Ed. 43 (2004) 3562–3565.
[31] A.V. Shlyakhtina, J.C.C. Abrantes, L.L. Larina, L.G. Shcherbakova, Solid State Ionics 176 (2005) 1653–1656.
[32] A.V. Shlyakhtina, O.K. Karyagina, L.G. Shcherbakova, Inorg. Mater. 40 (2004) 59–65.
[33] A.V. Shlyakhtina, A.V. Knotko, M.V. Boguslavskii, S.Y. Stefanovich, D.V. Peryshkov, I.V. Kolbanev, L.G. Shcherbakova, Solid State Ionics 176 (2005) 2297–2304.
[34] A.V. Shlyakhtina, A.V. Knot'ko, L.L. Larina, S.A. Borichev, L.G. Shcherbakova, Inorg. Mater. 40 (2004) 1312–1316.
[35] A.V. Shlyakhtina, A.V. Mosunov, S.Y. Stefanovich, A.V. Knotko, O.K. Karyagina, L.G. Shcherbakova, Inorg. Mater. 41 (2005) 264–271.
[36] A.V. Shlyakhtina, L.G. Shcherbakova, A.V. Knotko, Ferroelectrics 294 (2003) 175–190.
[37] A.V. Shlyakhtina, L.G. Shcherbakova, A.V. Knotko, A.V. Steblevskii, J. Solid State Electrochem. 8 (2004) 661–667.
[38] G.V. Shamrai, R.L. Magunov, L.V. Sadkovskaya, I.V. Stasenko, I.P. Kovalevskaya, Inorg. Mater. 27 (1991) 140–141.
[39] G.V. Shamrai, R.L. Magunov, I.V. Stasenko, A.P. Zhirnova, Inorg. Mater. 25 (1989) 233–235.
[40] G.V. Shamrai, R.L. Magunov, I.V. Stasenko, A.P. Zhirnova, Z. Neorg. Khim. 35 (1990) 798–800.
[41] G.V. Shamrai, A.V. Zagorodnyuk, R.L. Magunov, A.P. Zhirnova, Z. Neorga. Khim. 29 (1984) 3168–3170.
[42] G.V. Shamrai, A.V. Zagorodnyuk, R.L. Magunov, A.P. Zhirnova, Inorg. Mater. 28 (1992) 1633–1635.
[43] G.E. Sukhanova, K.N. Guseva, A.V. Kolesnikov, L.G. Shcherbakova, Inorg. Mater. 18 (1982) 1742–1745.
[44] A.V. Shlyakhtina, A.V. Mosunov, S.Y. Stefanovich, O.K. Karyagina, L.G. Shcherbakova, Inorg. Mater. 40 (2004) 1317–1320.
[45] G.C. Lau, R.S. Freitas, B.G. Ueland, B.D. Muegge, E.L. Duncan, P. Schiffer, R.J. Cava, Nat. Phys. 2 (2006) 249–253.
[46] M.A. Petrova, A.S. Novikova, R.G. Grebenshchikov, Dokl. Akad. Nauk Sssr. 246 (1979) 121–123.
[47] L.G. Shcherbakova, V.B. Glushkova, K.N. Guseva, L.G. Mamsurova, L.V. Sazonova, G.E. Sukhanova, Inorg. Mater. 16 (1980) 996–1000.
[48] J.L. Waring, S.J. Schneider, J. Res. Nat. Bur. Stand. Sec. A Phys. Chem. A 69 (1965) 255–261.
[49] M. Glerup, O.F. Nielsen, F.W. Poulsen, J. Solid State Chem. 160 (2001) 25–32.

[50] C. Heremans, B.J. Wuensch, J.K. Stalick, E. Prince, J. Solid State Chem. 117 (1995) 108–121.
[51] R.D. Shannon, C.T. Prewitt, Acta Crystallogra. B Struct. Crystallog. Crystal Chem. B 25 (1969) 925–946.
[52] S.T. Bramwell, M.N. Field, M.J. Harris, I.P. Parkin, J. Phys.-Conden. Matter 12 (2000) 483–495.
[53] M.J.P. Gingras, B.C. den Hertog, M. Faucher, J.S. Gardner, S.R. Dunsiger, L.J. Chang, B.D. Gaulin, N.P. Raju, J.E. Greedan, Phys. Rev. B. 62 (2000) 6496–6511.
[54] M.P. Zinkin, M.J. Harris, Z. Tun, R.A. Cowley, B.M. Wanklyn, J. Phys. Conden. Matter 8 (1996) 193–197.